

ORIGINAL RESEARCH

OPEN ACCESS



Tyk2 is a tumor suppressor in colorectal cancer

Stefan Moritsch^a, Bernadette Mödl^a, Irene Scharf^a, Lukas Janker^{b,c}, Daniela Zwolanek^a, Gerald Timelthaler^a, Emilio Casanova^d, Maria Sibilia^a, Thomas Mohr^a, Lukas Kenner^e, Dietmar Herndler-Brandstetter^a, Christopher Gerner^{b,c}, Mathias Müller^f, Birgit Strobl^f, and Robert Eferl^g

^aCenter for Cancer Research, Medical University of Vienna & Comprehensive Cancer Center, Vienna, Austria; ^bDepartment of Analytical Chemistry, Faculty of Chemistry, University of Vienna, Vienna, Austria; ^cJoint Metabolomics Facility, University and Medical University of Vienna, Vienna, Austria; ^dDepartment of Pharmacology, Center of Physiology and Pharmacology & Comprehensive Cancer Center, Medical University of Vienna, Vienna, Austria; ^eInstitute of Clinical Pathology, Medical University of Vienna, Vienna, Austria; ^fInstitute of Animal Breeding and Genetics, University of Veterinary Medicine Vienna, Vienna, Austria

ABSTRACT

Janus kinase Tyk2 is implicated in cancer immune surveillance, but its role in solid tumors is not well defined. We used Tyk2 knockout mice (Tyk2^{Δ/Δ}) and mice with conditional deletion of Tyk2 in hematopoietic (Tyk2^{ΔHem}) or intestinal epithelial cells (Tyk2^{ΔIEC}) to assess their cell type-specific functions in chemically induced colorectal cancer. All Tyk2-deficient mouse models showed a higher tumor burden after AOM-DSS treatment compared to their corresponding wild-type controls (Tyk2^{+/+} and Tyk2^{fl/fl}), demonstrating tumor-suppressive functions of Tyk2 in immune cells and epithelial cancer cells. However, specific deletion of Tyk2 in hematopoietic cells or in intestinal epithelial cells was insufficient to accelerate tumor progression, while deletion in both compartments promoted carcinoma formation. RNA-seq and proteomics revealed that tumors of Tyk2^{Δ/Δ} and Tyk2^{ΔIEC} mice were immunoevaded in different ways with downregulated and upregulated IFN γ signatures, respectively. Accordingly, the IFN γ -regulated immune checkpoint Ido1 was downregulated in Tyk2^{Δ/Δ} and upregulated in Tyk2^{ΔIEC} tumors, although both showed reduced CD8⁺ T cell infiltration. These data suggest that Tyk2^{Δ/Δ} tumors are Ido1-independent and poorly immunoevaded while Tyk2^{ΔIEC} tumors require Ido1 for immune evasion. Our study shows that Tyk2 prevents Ido1 expression in CRC cells and promotes CRC immune surveillance in the tumor stroma. Both of these Tyk2-dependent mechanisms must work together to prevent CRC progression.

ARTICLE HISTORY

Received 9 June 2022
Revised 15 September 2022
Accepted 15 Sep 2022

KEYWORDS

colitis-associated colorectal cancer; azoxymethane AOM; dextran sulfate salt DSS; indoleamine 2; 3-dioxygenase 1 Ido1; interferon gamma

Introduction



Colorectal cancer (CRC) is the third leading cause of cancer-related death in males and females.¹ Most patients develop sporadic CRC, but approximately 2% suffer from colitis-associated CRC. In particular, patients with inflammatory bowel diseases (IBD) such as ulcerative colitis (UC) or Crohn's disease (CD) have a threefold increased risk of developing CRC.^{2–5} The genetic and epigenetic basis of CRC has been well studied, and accurate treatment options have reduced mortality of CRC patients over the past few decades.¹ However, treatment of metastatic CRC is still challenging, and new therapies are needed.


The best-characterized oncogenic signaling pathways are the RAS mitogen-activated protein kinase (MAPK) and phosphatidylinositol-3-kinase (PI3K) AKT pathways.^{6–9} In recent years, the Janus kinase signal transducer and activator of transcription (Jak-Stat) signaling pathway is increasingly considered crucial for development of various cancer types.^{10,11} Jak-Stat signaling is activated by cytokines, and corresponding receptors are expressed in cancer cells and immune cells.^{12,13} Therefore, Jak-Stat signaling not only mediates cancer cell-intrinsic functions but also orchestrates immune responses in

the tumor microenvironment.¹⁴ When cytokines bind to their cognate receptors, Jaks are activated and phosphorylate-specific tyrosine residues in the intracellular receptor domains. This creates docking sites for Stat proteins that bind to the receptor and are tyrosine-phosphorylated by Jaks. The activated Stats dimerize, translocate to the nucleus, and regulate transcription of target genes involved in cell proliferation, apoptosis, cell differentiation and immunological processes.¹⁵ The Jak-Stat families consist of four Jaks (Jak1, Jak2, Jak3, Tyk2) and seven Stats (Stat1, Stat2, Stat3, Stat4, Stat5a, Stat5b, Stat6).

Interferons (IFNs) activate Stat1 and Stat2 via Jak1, Jak2 and Tyk2, while members of the IL-6 family activate Stat3 via gp130-associated Jak1, Jak2 and to some extent Tyk2.^{15,16} In addition, Tyk2 is activated by type I IFNs, IL-10 and IL-12 cytokine families but not by IFN γ . Although Tyk2 can activate all Stat proteins, it cannot transmit cytokine signals itself but requires Jak1 or Jak2 as a partner.^{16–18}

Jak-Stat signaling plays a dual role in carcinogenesis. Chromosomal Jak translocations leading to constitutive activation of multiple oncogenic signaling pathways have been identified in hematological malignancies.^{19,20} In addition,

CONTACT Robert Eferl  robert.eferl@meduniwien.ac.at  Center for Cancer Research, Medical University of Vienna & Comprehensive Cancer Center, 1090 Vienna, Austria

 Supplemental data for this article can be accessed online at <https://doi.org/10.1080/2162402X.2022.2127271>

© 2022 The Author(s). Published with license by Taylor & Francis Group, LLC.

This is an Open Access article distributed under the terms of the Creative Commons Attribution License (<http://creativecommons.org/licenses/by/4.0/>), which permits unrestricted use, distribution, and reproduction in any medium, provided the original work is properly cited.

activating mutations in Jak2 and Stat3 have been found in leukemias and solid cancers.²¹ In contrast, Stat1 is considered a tumor suppressor as it regulates expression of pro-apoptotic and anti-proliferative genes as well as molecules of the antigen presentation machinery, which increases tumor immunogenicity.^{22–24} A dual role of Jak-Stat signaling has also been observed in CRC. An oncogenic function of epithelial IL-6-Stat3 signaling was identified in the azoxymethane–dextran sulfate salt (AOM-DSS) mouse model of colitis-associated CRC.²⁵ In the sporadic Apc^{Min} CRC model, Stat3 had a tumor-suppressive function in cancer cells and prevented epithelial-to-mesenchymal transition (EMT) and invasiveness.²⁶ Similarly, a tumor-suppressive function of epithelial Stat1 was found in the AOM-DSS CRC model, but only in male mice.²⁷ In Apc^{Min} mice, epithelial Stat1 had an oncogenic function and promoted the formation of Ido1-expressing cancer cells that mediated immune escape.²⁸

The role of Tyk2 in carcinogenesis is not well defined. Oncogenic Tyk2 mutations have been found in leukemias,^{29–34} and several cancer types such as squamous cell carcinoma and prostate cancer exhibit Tyk2 activation.^{35–37} However, loss-of-function (LOF) mutations have also been described in breast, gastric and colon cancer.³⁸ In this study, we examined tumor cell-intrinsic and extrinsic functions of Tyk2 in CRC. Our data revealed tumor-suppressive functions of Tyk2 in cancer cells as well as immune cells of the tumor microenvironment.

Results

Tyk2 deficiency promotes CRC formation

We used Tyk2^{Δ/Δ} mice with a Tyk2 germline deletion, Tyk2^{ΔIEC} mice (Tyk2^{fl/fl} Villin-cre) with specific deletion of Tyk2 in the intestinal epithelium and Tyk2^{ΔHem} mice (Tyk2^{fl/fl} Vav-cre) with specific deletion of Tyk2 in hematopoietic cells to study cancer cell-intrinsic and extrinsic functions of Tyk2 in CRC. We confirmed tissue-specific deletion of Tyk2 in these mouse strains by PCR analysis of DNA isolated from different organs and IECs (Supplementary Figure 1a). Tyk2 was completely deleted from the IECs of Tyk2^{ΔIEC} mice. Weak deletion was observed in the kidney, which is consistent with published results.²⁶ Tyk2 was also completely deleted in the spleen of Tyk2^{ΔHem} mice, which consists mainly of hematopoietic cells, and partially deleted in other organs, most likely due to the presence of immune cells. As expected, deletion was complete in all organs of Tyk2^{Δ/Δ} mice. Different staining protocols were employed in Tyk2^{ΔIEC} and Tyk2^{Δ/Δ} mice to investigate whether epithelial or complete deletion of Tyk2 affects expression of Stat1 and Stat3 proteins as well as colonic homeostasis. Immunohistochemistry (IHC) showed unaltered numbers of Stat1⁺ colonic epithelial cells and lamina propria cells in Tyk2^{ΔIEC} and Tyk2^{Δ/Δ} mice (Supplementary Figure 1b,c). Stat3⁺ colonic epithelial cells and lamina propria cells were increased in Tyk2^{Δ/Δ} but not in Tyk2^{ΔIEC} mice (Supplementary Figure 1d,e). No marked activation of Stat1 and Stat3 could be observed in both cell compartments (Supplementary Figure 1b–e). Proliferating cells in the crypts and enteroendocrine cells were unchanged (Supplementary

Figure 1f, g), while the number of goblet cells was slightly increased in Tyk2^{Δ/Δ} mice (Supplementary Figure 1f). These data show that specific deletion of Tyk2 in IECs has no effect on Stat1 and Stat3 expression and activation and does not affect secretory cell differentiation and crypt proliferation in the colon. However, complete deletion of Tyk2 increased Stat3 expression and promoted goblet cell differentiation to some extent.

To investigate the role of Tyk2 in the development of CRC, we applied the AOM – DSS protocol for colitis-associated CRC to Tyk2^{ΔIEC}, Tyk2^{ΔHem} and Tyk2^{Δ/Δ} mice. Macroscopic and histologic analysis of formalin-fixed colon tissues (Figure 1a) revealed increased tumor burden in all three Tyk2-deficient mouse strains (Figure 1d, h, l). Tyk2^{ΔIEC} mice developed larger tumors, whereas tumor multiplicity was unchanged (Figure 1f, g). In contrast, Tyk2^{ΔHem} mice developed more tumors, but the size was unchanged (Figure 1j, k). In Tyk2^{Δ/Δ} mice, both multiplicity and size were increased (Figure 1b, c). Furthermore, tumor progression was analyzed according to several histopathologic criteria (Supplementary Figure 2a). Increased numbers of high-grade adenomas and carcinomas were found in Tyk2^{Δ/Δ} mice but not in Tyk2^{ΔIEC} or Tyk2^{ΔHem} mice (Figure 1e,i,m). To investigate whether deletion of Tyk2 in epithelial cells has an impact on the severity of chronic colitis, we monitored the body weights of Tyk2^{fl/fl} and Tyk2^{ΔIEC} mice during the course of AOM-DSS treatment. We found a trend of increased weight loss in Tyk2^{ΔIEC} mice after the first cycle of DSS, while weight loss decreased after the second cycle, indicating that there is no difference in overall colitis severity (Supplementary Figure 2b). These data demonstrate that Tyk2 is a tumor suppressor in both cancer cell and immune cell compartments of CRC. Combined Tyk2 deletion in cancer cells and cells of the tumor stroma promotes CRC progression to invasive carcinomas.

Differential interferon signatures in Tyk2^{ΔIEC} and Tyk2^{Δ/Δ} tumors

Our data indicate additive tumor-suppressive functions of Tyk2 in epithelial cancer cells and stromal cells. To elucidate these functions, we performed RNA-seq analysis with tumor RNA from Tyk2^{ΔIEC} and Tyk2^{Δ/Δ} mice. Principal component analyses of RNA-seq data showed that tumors from Tyk2^{Δ/Δ} and Tyk2^{ΔIEC} mice differed from their Tyk2^{fl/fl} and Tyk2^{+/+} littermate controls (Figure 2a,b). We found 288 genes in Tyk2^{Δ/Δ} tumors and 399 genes in Tyk2^{ΔIEC} tumors that were differentially expressed at least twofold when compared to corresponding controls (Supplementary Tables 1–4). Surprisingly, Tyk2 was not among the top hits of differentially expressed genes. The floxed sequence in the targeted Tyk2 allele includes exon 3, which contains the start codon for Tyk2 protein translation. We reasoned Tyk2 deletion still results in RNA transcripts that do not yield protein but generate signals during RNA-seq analysis. Therefore, we analyzed the RNA-seq data with the Integrated Genome Viewer software (Supplementary Figure 3a). This analysis revealed a significant number of aligned reads in Tyk2 genomic regions of Tyk2^{Δ/Δ} and Tyk2^{ΔIEC} tumors. However, exon 3 reads were completely absent in Tyk2^{Δ/Δ} tumors and most Tyk2^{ΔIEC}

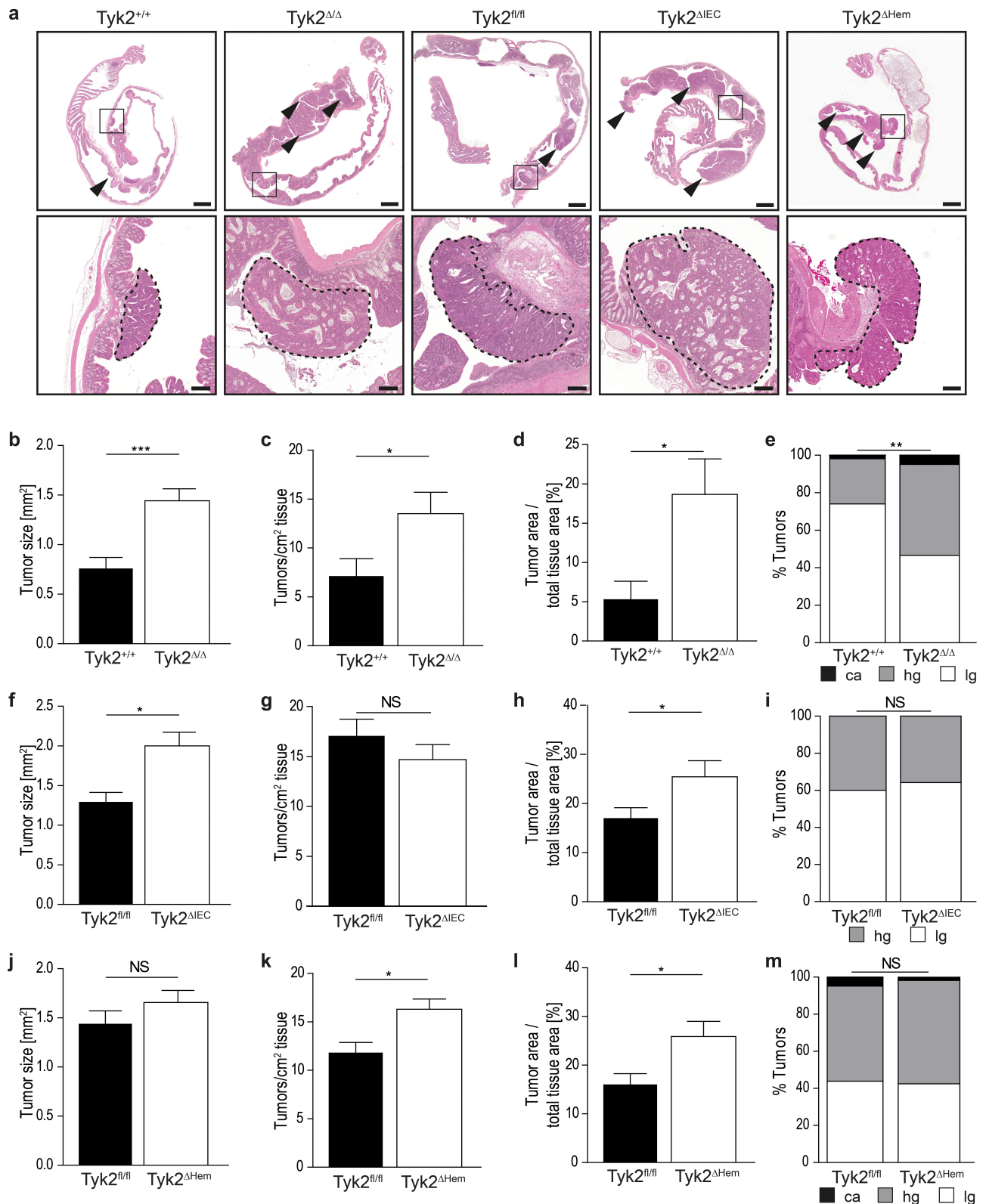


Figure 1. Increased colonic tumor burden in AOM-DSS-treated Tyk2^{Δ/Δ}, Tyk2^{ΔIEC} and Tyk2^{ΔHem} mice. (a) H/E-stained colons from Tyk2^{+/+}, Tyk2^{Δ/Δ}, Tyk2^{fl/fl}, Tyk2^{ΔIEC} and Tyk2^{ΔHem} mice demonstrating the increased number of colonic tumors (arrowheads) after AOM-DSS treatment in Tyk2-deficient mice. Scale bars indicate 2000 μm in the overview and 200 μm in the zoomed in portion. (b–e) Evaluation of tumor parameters and tumor grading in AOM-DSS treated Tyk2^{Δ/Δ} mice. Quantification of tumor size ($n \geq 54$ tumors per genotype) (b), tumor multiplicity ($n \geq 7$ mice per genotype) (c) and tumor load ($n \geq 7$ mice per genotype) (d) in Tyk2^{Δ/Δ} compared to littermate controls. Tumor grading of colonic tumors in AOM-DSS treated Tyk2^{Δ/Δ} ($n \geq 54$ tumors per genotype) (e). (f–i) Evaluation of tumor parameters and tumor grading in AOM-DSS treated Tyk2^{ΔIEC} mice. Quantification of tumor size ($n \geq 278$ tumors per genotype) (f), tumor multiplicity ($n \geq 18$ mice per genotype) (g) and tumor load ($n \geq 18$ mice per genotype) (h) in Tyk2^{ΔIEC} compared to littermate controls. Tumor grading of colonic tumors in AOM-DSS treated Tyk2^{ΔIEC} ($n \geq 278$ tumors per genotype) (i). (j–m) Evaluation of tumor parameters and tumor grading in AOM-DSS treated Tyk2^{ΔHem} mice. Quantification of tumor size ($n \geq 84$ tumors per genotype) (j), tumor multiplicity ($n \geq 8$ mice per genotype) (k) and tumor load ($n \geq 8$ mice per genotype) (l) in Tyk2^{ΔHem} compared to littermate controls. Tumor grading of colonic tumors in AOM-DSS-treated Tyk2^{ΔHem} ($n \geq 84$ tumors per genotype) (m). Graphs depicting the tumor size (b, f, j), are based on data from individual tumors. Tumor load (d, h, l) was calculated as tumor area per total tissue area in %. ca: carcinoma, hg: high grad adenoma, lg: low grade adenoma. Bars represent mean \pm SEM. Statistical tests: Mann-Whitney test for tumor size, unpaired *t*-test for tumor multiplicity and tumor load, χ^2 -test for tumor grading. NS: not significant, * $p < .05$, ** $p < .01$, *** $p < .001$.

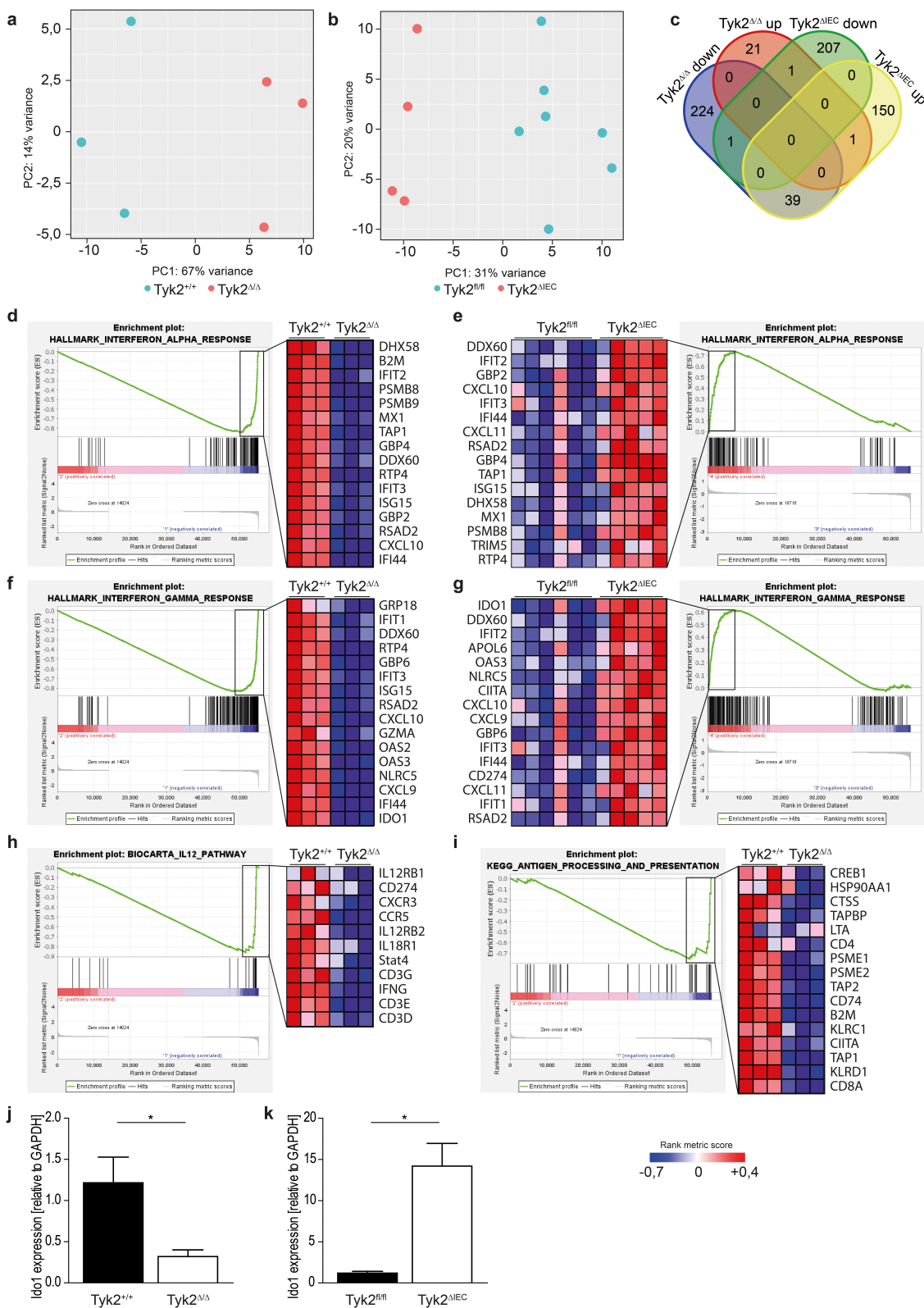


Figure 2. Oposing effects of epithelial and stromal Tyk2 deficiencies on IFN γ signaling. (a, b) Principal component analysis of AOM-DSS induced tumors in $Tyk2^{+/+}$, $Tyk2^{\Delta/\Delta}$ (a) $Tyk2^{fl/fl}$ and $Tyk2^{\Delta/IEC}$ (b) mice showing that tumors from $Tyk2^{\Delta/\Delta}$ and $Tyk2^{\Delta/IEC}$ mice are distinctly different from their respective controls. (c) Venn diagram of differentially expressed genes in $Tyk2^{\Delta/\Delta}$ and $Tyk2^{\Delta/IEC}$ tumors depicting an overlap of 39 genes between downregulated genes in AOM-DSS induced tumors of $Tyk2^{\Delta/\Delta}$ mice and downregulated genes of tumors of $Tyk2^{\Delta/IEC}$ mice. (d–i) Gene set enrichment analysis of the “Interferon Alpha Response” (d, e), “Interferon Gamma Response” (f, g), “IL12 pathway” (h) and “Antigen Processing and Presentation” (i) gene sets in $Tyk2^{\Delta/\Delta}$ (d, f, h, i) and $Tyk2^{\Delta/IEC}$ (e, g) tumors showing the leading edge of the enriched genes. (j, k) qPCR analysis of Ido1 expression in $Tyk2^{\Delta/\Delta}$ (j) and $Tyk2^{\Delta/IEC}$ (k) tumors compared to $Tyk2^{+/+}$ and $Tyk2^{fl/fl}$ respectively. $Tyk2^{+/+}$ and $Tyk2^{\Delta/\Delta}$: $n = 3$ pooled tumor samples per genotype, $Tyk2^{fl/fl}$ and $Tyk2^{\Delta/IEC}$: $n \geq 4$ pooled tumor samples per genotype. Bars represent mean \pm SEM. Statistical test: unpaired t -test. * $p < .05$.

tumors. Quantitative PCR (qPCR) analysis for Tyk2 mRNA expression using primers in exon 3 confirmed these data and showed absent and greatly reduced expression in Tyk2 Δ/Δ and Tyk2 Δ/IEC tumors, respectively (Supplementary Figure 3b).

Since tumor burden was increased in Tyk2 Δ/Δ and Tyk2 Δ/IEC mice, we expected similar sets of differentially expressed genes in Tyk2 Δ/Δ and Tyk2 Δ/IEC tumors. However, little overlap was observed with Ccl7 as the only commonly downregulated and Pkd11l1 as the only commonly upregulated gene (Figure 2c, Supplementary Figure 3c-e). Pde11a was upregulated in Tyk2 Δ/Δ and downregulated in Tyk2 Δ/IEC tumors. Thirty-nine genes were downregulated in Tyk2 Δ/Δ and upregulated in Tyk2 Δ/IEC tumors. Most of these genes respond to interferon (IFN) signaling. They include members of the antigen processing and presentation machinery (Tap1), several type I interferon-stimulated genes (Ifi1-3, Ifi44, Oas3), H-2 major histocompatibility complex class I antigens (H2-Q5/Q7/Q9/T10), the immune checkpoint PD-L1 as well as genes involved in metabolic processes (Apol6, Apol9, Apol10, Ido1) (Supplementary Figure 3c-e). Using the Gene Set Enrichment Analysis tool of the Broad Institute,^{39,40} we found that gene sets correlating with IFN α and IFN γ responses were negatively enriched in Tyk2 Δ/Δ tumors and positively enriched in Tyk2 Δ/IEC tumors (Figure 2d-g). IFN γ production is mainly regulated by IL12. Consequently, the gene set for IL12 signaling containing IFN γ was also negatively enriched in Tyk2 Δ/Δ tumors (Figure 2h) but not in Tyk2 Δ/IEC tumors (Supplementary Tables 3 and 4). Similarly, the IFN γ -dependent gene signature for antigen processing and presentation was negatively enriched in Tyk2 Δ/Δ tumors (Figure 2i) but not in Tyk2 Δ/IEC tumors (Supplementary Tables 3 and 4). Deregulation of key genes identified in the RNA-seq analysis was confirmed by qPCR (Supplementary Figure 3f, g). These data suggest that IFN-mediated immune functions are severely impaired in Tyk2 Δ/Δ tumors, while Tyk2 Δ/IEC tumors exhibit enhanced IFN signatures. Therefore, the increased tumor burden in Tyk2 Δ/Δ and Tyk2 Δ/IEC mice is due to different molecular mechanisms.

Increased Ido1 protein expression in Tyk2 Δ/IEC tumors

In particular, the differentially regulated Ido1 gene caught our attention in the RNA-seq dataset because it encodes for the enzyme indolamin-2,3-dioxygenase, which has immune-suppressive functions in various cancer types including CRC.⁴¹⁻⁴³ As expected from the enrichment plots for IFN γ signaling, Ido1 mRNA expression was downregulated in Tyk2 Δ/Δ tumors and upregulated in Tyk2 Δ/IEC tumors (Figure 2f,g, Supplementary Figure 3c-e). We confirmed this finding by qPCR analysis (Figure 2j,k). Furthermore, qPCR showed that Ido1 was downregulated in Tyk2 Δ/Hem tumors similar to Tyk2 Δ/Δ tumors (Supplementary Figure 3h). However, it is not clear whether these changes RNA expression are reflected by differential protein expression. Therefore, proteomics from Tyk2 Δ/Δ and Tyk2 Δ/IEC tumor tissues was performed. Thirty-three downregulated proteins were identified in Tyk2 Δ/Δ tumors compared to Tyk2 $^{+/+}$ tumors that are associated with antigen processing and presentation, IFN signaling and immune responses (Figure 3a-c). The corresponding genes

of most of these proteins were also differentially expressed (Figure 2, Supplementary Figure 3c-e, Supplementary Tables 1 and 2). In Tyk2 Δ/IEC tumors, 8 downregulated and 13 upregulated proteins were identified when compared to Tyk2 $^{fl/fl}$ tumors (Figure 3d-f). While downregulated proteins were mainly implicated in protein turnover and metabolic processes, upregulated proteins were involved in DNA replication, cell cycle regulation, and extracellular matrix organization. Most genes encoding these proteins showed less than two-fold deregulation in the RNA-seq dataset, indicating post-transcriptional regulation (Supplementary Tables 3 and 4). Similarly, only a few IFN γ -regulated genes identified by RNA-seq (Figure 2e) were also significantly deregulated at the protein level in Tyk2 Δ/IEC tumors. Importantly, the Ido1 protein was the top hit in both Tyk2 Δ/Δ and Tyk2 Δ/IEC tumors. Consistent with the RNA-seq data, the Ido1 protein was downregulated in Tyk2 Δ/Δ tumors and upregulated in Tyk2 Δ/IEC tumors (Figure 3a-f). These data indicate that Ido1-dependent immune suppression is reduced in Tyk2 Δ/Δ tumors but enhanced in Tyk2 Δ/IEC tumors.

Increased Ido1-expressing Paneth-like cancer cells in Tyk2 Δ/IEC tumors

Ido1-derived metabolites promote immunosuppression and T cell anergy.⁴³ We recently showed in intestinal tumors of Apc $^{\text{Min}}$ mice that Ido1 is predominantly expressed by Mmp7 $^+$ Paneth-like cancer cells in an IFN γ /Stat1-dependent manner.²⁸ Therefore, we performed immunofluorescence (IF) staining for Mmp7 and Ido1 in Tyk2 Δ/Δ and Tyk2 Δ/IEC tumors (Figure 4a, b). Mmp7 $^+$ Paneth-like cancer cells were present in Tyk2 Δ/Δ , but they did not express Ido1. Furthermore, Ido1 expression was blunted in stromal cells of Tyk2 Δ/Δ tumors (Figure 4a,c). In contrast, Tyk2 Δ/IEC tumors contained an increased number of Ido1-expressing cancer cells when compared to Tyk2 $^{fl/fl}$ controls. Most of these cells were also positive for the Paneth cell marker Mmp7. Stromal Ido1 expression was unaltered in Tyk2 Δ/IEC tumors (Figure 4b,d). These data indicate that Tyk2 impairs Ido1 expression in Paneth-like cancer cells of CRC, which is induced by stromal signals.

Reduced antitumor immune cell infiltration in Tyk2 Δ/Δ and Tyk2 Δ/IEC tumors

The presence of Ido1-expressing Paneth-like cancer cells was associated with increased tumor burden and reduced T-cell infiltration in tumors of Apc $^{\text{Min}}$ mice, while no correlation with tumor cell proliferation or apoptosis was observed.²⁸ We expected a similar phenotype in Tyk2 Δ/IEC tumors and characterized tumor parameters, Stat expression, and immune cell infiltration by IHC and FACS analyses. IHC analysis revealed similar numbers of proliferating BrdU $^+$ and apoptotic cleaved caspase3 $^+$ tumor cells in Tyk2 Δ/Δ and Tyk2 Δ/IEC tumors when compared to Tyk2 $^{+/+}$ and Tyk2 $^{fl/fl}$ controls (Supplementary Figure 4a-d). Stat1 expression and activation were reduced in cancer cell and stromal cell compartments of Tyk2 Δ/Δ tumors, respectively (Supplementary Figure 4e, g), whereas Stat3 expression and activation remained unchanged (Supplementary Figure 4i, k). In contrast, expression of Stat1

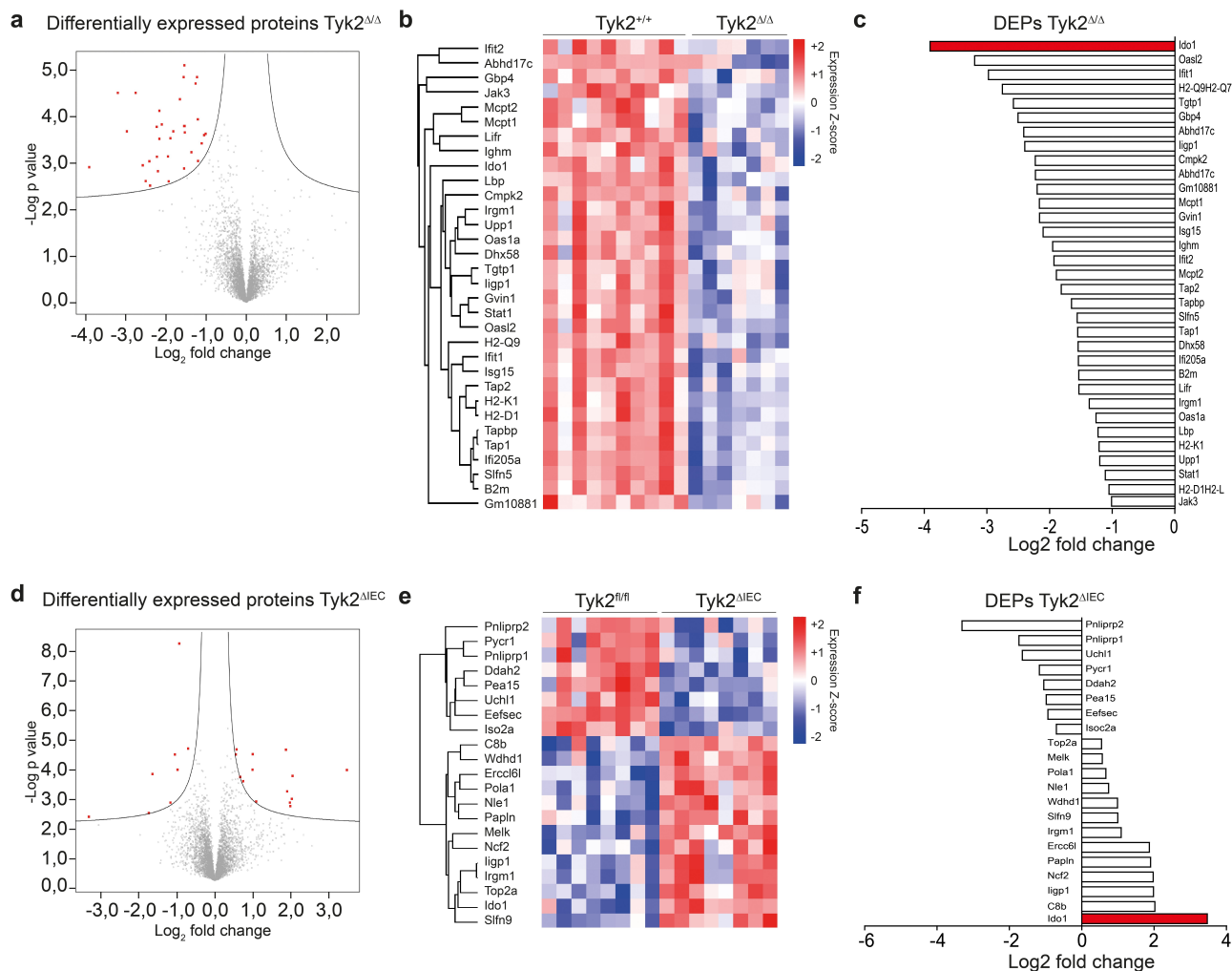


Figure 3. Oposing effects of epithelial and stromal $Tyk2$ deficiencies on $Ido1$ protein expression. (a-f) Analysis of differentially expressed proteins (DEPs) in AOM-DSS induced colonic tumors of $Tyk2^{\Delta/\Delta}$ and $Tyk2^{\Delta IEC}$ mice compared to their respective controls. Volcano plot (a), heatmap (b) and relative quantification (c) of DEPs in AOM-DSS induced colonic tumors of $Tyk2^{\Delta/\Delta}$ mice ($n \geq 7$ tumors per genotype). Volcano plot (d), heatmap (e) and relative quantification (f) of DEPs in AOM-DSS induced colonic tumors of $Tyk2^{\Delta IEC}$ mice ($n \geq 7$ tumors per genotype).

was increased in cancer cells of $Tyk2^{\Delta IEC}$ tumors (Supplementary Figure 4f) while expression of $Stat3$ and activation of $Stat1$ and $Stat3$ were not altered (Supplementary Figure 4h, j, l).

We next assessed immune cell infiltration into $Tyk2^{\Delta/\Delta}$ and $Tyk2^{\Delta IEC}$ tumors. The extent of stromalization and the number of $CD45^+$ cells in the tumor stroma were not altered in $Tyk2^{\Delta/\Delta}$ and $Tyk2^{\Delta IEC}$ tumors (Supplementary Figure 5a-c, e, j). However, IHC and FACS analysis revealed reduced infiltration of NK cells and $CD3^+$ T cells (Figure 5a,b, Supplementary Figure 5c,f,g) as well as $CD8^+$ T cells in $Tyk2^{\Delta/\Delta}$ tumors, while infiltration of $CD4^+$ T cells was unchanged (Figure 5c, d, Supplementary Figure 5c, h, i) and Tregs were increased (Figure 5e, Supplementary Figure 5d). In $Tyk2^{\Delta IEC}$ tumors, infiltration of $NK1.1^+$ NK cells and Tregs ($Tyk2^{+/+}$: $1,830 \pm 0,7238$, $n = 4$; $Tyk2^{\Delta/\Delta}$: $1,616 \pm 0,3618$, $n = 5$) was unchanged but $CD3^+$, $CD4^+$ and $CD8^+$ T cells were reduced (Figure 5f-i, Supplementary Figure 5c, k-n). Additional FACS analysis for $PD-1^+$ T cell populations showed a trend of $CD8^+$ T cell exhaustion in $Tyk2^{\Delta/\Delta}$ and $Tyk2^{\Delta IEC}$ tumors, but this was

not significant (Supplementary Figure 5c, o, p). The data demonstrate that $CD3^+$ and $CD8^+$ T cell infiltration is impaired in $Tyk2^{\Delta/\Delta}$ and $Tyk2^{\Delta IEC}$ tumors, which may reduce cancer immune surveillance and lead to increased tumor load. In contrast to $Tyk2^{\Delta/\Delta}$ and $Tyk2^{\Delta IEC}$ tumors, $CD3^+$ and $CD8^+$ T cell infiltration was not impaired in $Tyk2^{\Delta Hem}$ tumors. However, $FoxP3^+$ cells were increased while Granzyme B⁺ cells were decreased (Supplementary Figure 6a-e), which may also reduce cancer immune surveillance and lead to increased tumor multiplicity. The data from $Tyk2^{\Delta Hem}$ tumors suggest that deletion of $Tyk2$ in cancer cells is required for reduced $CD8^+$ T cell infiltration.

Discussion

The role of $Tyk2$ in solid tumors is not well defined and oncogenic as well as tumor-suppressive functions have been reported. Here, we show that $Tyk2$ is a tumor suppressor in CRC. Using three different mouse models with $Tyk2$ deletion and the AOM-DSS protocol for colitis-associated CRC, we

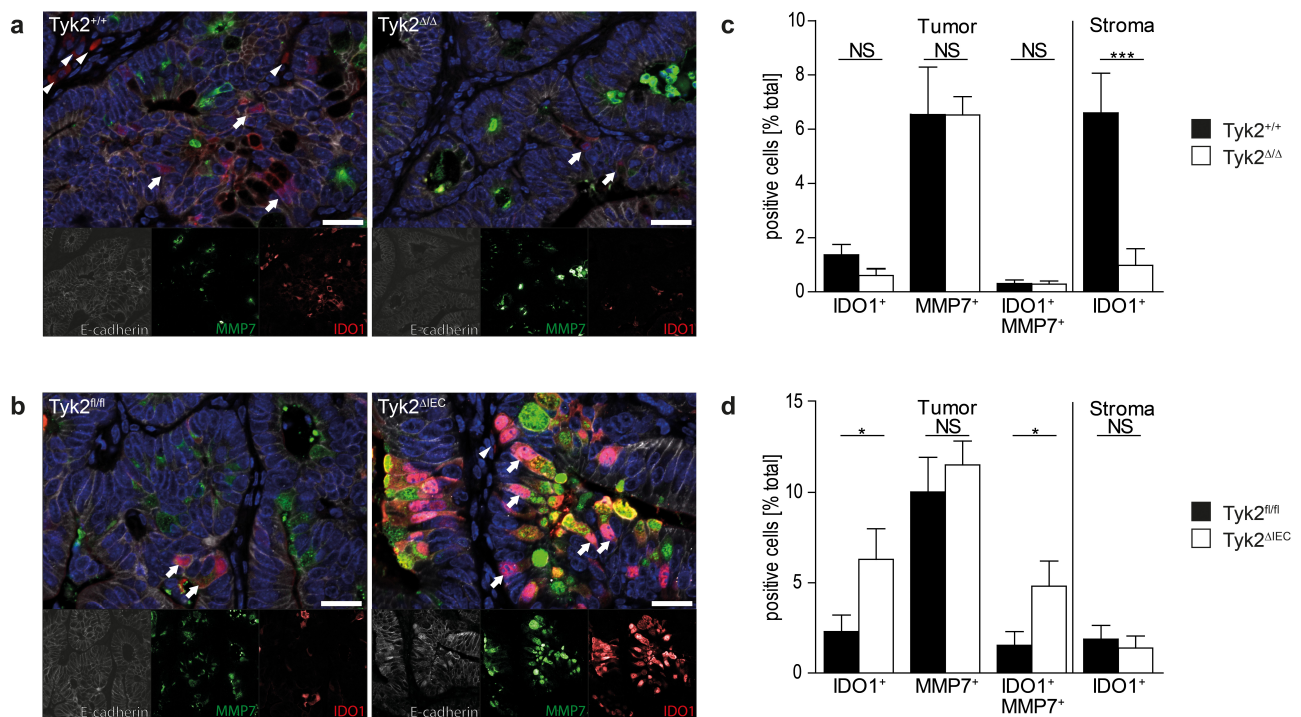


Figure 4. Increased numbers of IdO1 by Paneth-like cells in AOM-DSS-induced colonic tumors of Tyk2^{ΔIEC} mice. (a–d) Investigation of IDO1 expression and activity in AOM-DSS-induced colonic tumors of Tyk2^{Δ/Δ} and Tyk2^{ΔIEC} mice. IF stainings (a, b) and quantification (c, d) of IDO1-expressing tumor cells (arrows) and stromal cells (arrowheads) in colonic tumors of Tyk2^{+/+} and Tyk2^{Δ/Δ} ($n \geq 11$ tumors in $n = 3$ animals per genotype) (a, c) and Tyk2^{fl/fl} and Tyk2^{ΔIEC} ($n \geq 10$ tumors in $n = 3$ animals per genotype) (b, d) mice; Scale bars represent 20 μm . Bars represent mean \pm SEM. NS: not significant. Statistical test: unpaired *t*-test. * $p < .05$, *** $p < .001$.

demonstrate additive tumor-suppressive functions of Tyk2 in cancer cells and in the immune microenvironment. Tyk2 deletion in cancer cells or in immune cells increased the tumor burden, but only combined deletion in both cellular compartments promoted tumor progression. The qualitative differences in tumor formation in the three mouse models could be due to differential infiltration and activation of immune cells modulated by loss of Tyk2 in both the hematopoietic system and the epithelial cancer cell compartment. Our data also suggest that the use of Tyk2 inhibitors to treat IBD, which is currently being investigated in clinical trials, should be viewed with caution as it blocks Tyk2 in all cell types and could promote progression of as yet unrecognized neoplastic lesions.

There is ample evidence that Tyk2 is involved in immune surveillance of cancer.^{44–46} Tyk2 is required for IL12 production by myeloid cells, which triggers a Th1 response with enhanced IFN γ production and tumor cell killing by CD8⁺ T cells and NK cells.⁴⁷ Therefore, we expected similar cancer phenotypes in Tyk2^{Δ/Δ} and Tyk2^{ΔHem} mice since both mouse models lack Tyk2 in immune cells. However, Tyk2^{Δ/Δ} mice developed significantly larger and more aggressive tumors, while the increase in tumor burden in Tyk2^{ΔHem} mice was rather subtle. Only tumor multiplicity was increased, suggesting that hematopoietic Tyk2 is involved in early immune surveillance of CRC but not in tumor progression. Interestingly, Tyk2^{Δ/Δ} and Tyk2^{ΔIEC} tumors showed a similar reduction of CD8⁺ T cell infiltration that was not found in Tyk2^{ΔHem} tumors. This indicates that Tyk2 deletion in the epithelial cancer cell compartment is responsible for reduced infiltration of CD8⁺ T cells into tumors.

While the importance of Tyk2 in cancer immune surveillance is well established, there is little evidence of Tyk2 functions in cancer cells.⁴⁶ Tyk2 has been shown to drive human cancer cell invasion and metastasis in a cancer cell-intrinsic manner.¹⁴ The AOM-DSS model does not allow assessment of metastasis, but comparison of tumor data in Tyk2^{Δ/Δ} and Tyk2^{ΔIEC} mice rather suggest an anti-metastatic function of Tyk2 in cancer cells, which becomes evident when Tyk2-mediated immune surveillance is impaired. We recently showed that Tyk2 mediates protective IL22 signaling in gut epithelial cells during DSS-induced acute colitis.⁴⁸ We did not observe increased lethality of Tyk2^{Δ/Δ}, Tyk2^{ΔHem} or Tyk2^{ΔIEC} mice during DSS-induced induction of chronic colitis in the AOM-DSS protocol. Furthermore, gene expression data provided no evidence of impaired IL22 signaling and tumor proliferation rates were unaffected, suggesting that cancer phenotypes are IL22-independent.

The RNA-seq and proteomics data revealed different molecular profiles of Tyk2^{Δ/Δ} and Tyk2^{ΔIEC} tumors. We found deregulated proteins also in the RNA-seq dataset, but most candidates were less than two-fold deregulated at the transcriptional level. Therefore, we hypothesize that post-transcriptional processes are strongly involved in the deregulation of proteins. Consistently, Tyk2 has previously been shown to be involved in the regulation of translation.⁴⁹ Most differentially expressed genes and proteins were part of an IFN signature and were regulated in opposite directions in Tyk2^{Δ/Δ} and Tyk2^{ΔIEC} tumors suggesting differential cancer genesis and immunoediting. However, it remains unclear how cancer cell-specific Tyk2 deletion can lead to increased IFN signaling

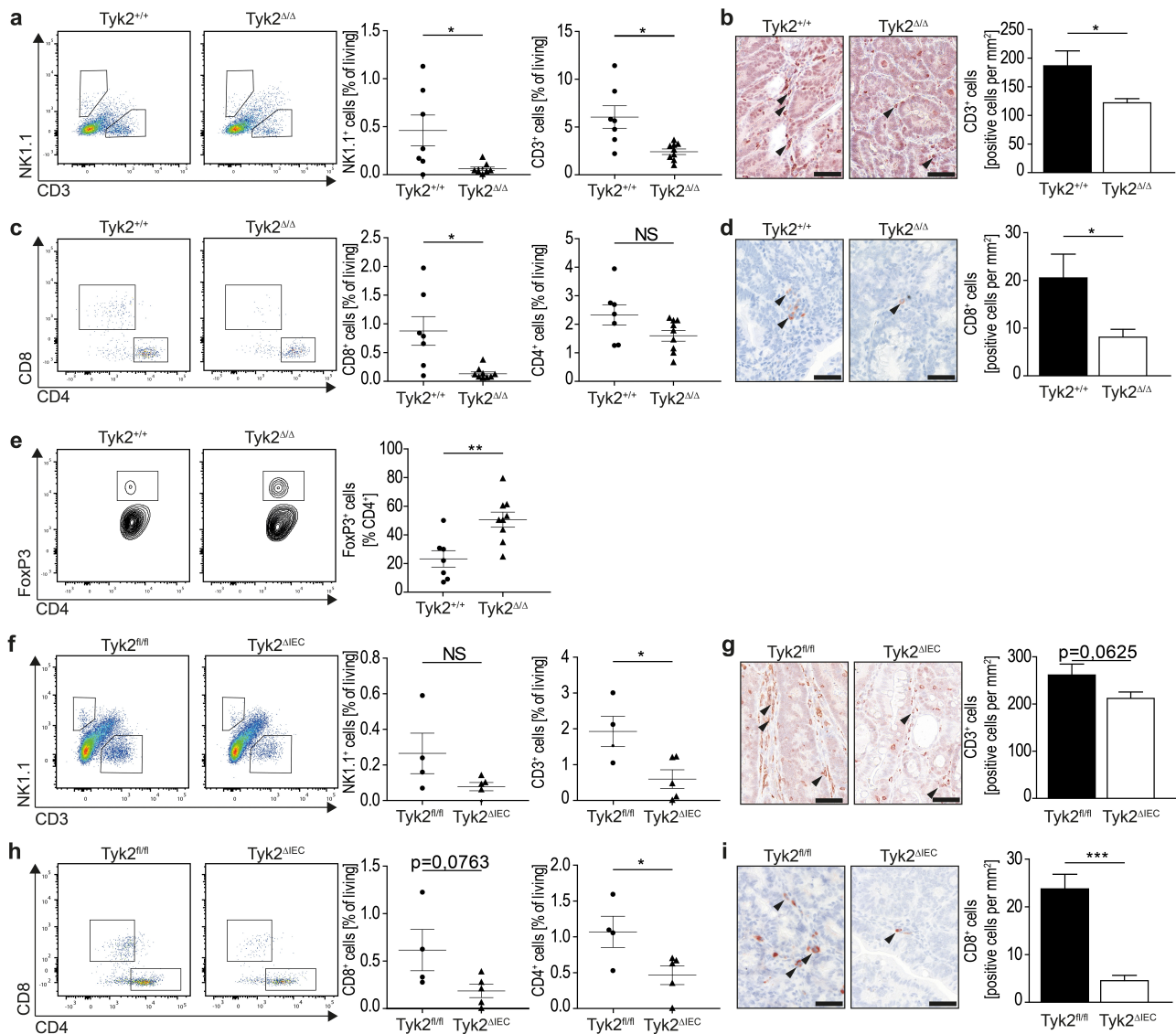


Figure 5. Analysis of immune cell infiltration in the tumor stroma of AOM-DSS-induced colonic tumors of Tyk2^{Δ/Δ} and Tyk2^{ΔIEC} mice. (a–h) Analysis of immune cell infiltration in AOM-DSS induced colonic tumors in Tyk2^{Δ/Δ} (a–e) and Tyk2^{ΔIEC} (f–i) mice using flow cytometry and IHC. FACS plots and quantification of NK1.1⁺ NK cell and CD3⁺ Lymphocyte infiltration ($n \geq 4$ animals per genotype, tumors from each mouse were pooled) (a, f). IHC staining and quantification of CD3⁺ Lymphocytes (arrowheads) ($n \geq 20$ tumors in $n \geq 4$ animals per genotype), Scale bars indicate 50 μ m (b, g). FACS plots and quantification of CD4⁺- and CD8⁺ T-Lymphocyte infiltration ($n \geq 4$ animals per genotype, tumors from each mouse were pooled) (c, h). IHC staining and quantification of CD8⁺ T-Lymphocytes (arrowheads) ($n \geq 29$ tumors in $n \geq 3$ animals per genotype), Scale bars indicate 50 μ m (d, i). FACS plots and quantification of CD4⁺FoxP3⁺ T-Lymphocyte infiltration ($n \geq 7$ animals per genotype, tumors from each mouse were pooled) (e). Bars represent mean \pm SEM. Statistical tests: unpaired *t*-test for Tyk2^{Δ/Δ} data and Tyk2^{ΔIEC} IHC data, Mann–Whitney test for Tyk2^{ΔIEC} FACS data. NS: not significant, * $p < .05$, ** $p < .01$, *** $p < .001$.

as seen in Tyk2^{ΔIEC} tumors. Although IFN γ plays a key role in cancer immune surveillance, sustained activity can result in upregulation of immune checkpoints that promote immune evasion.⁵⁰ We found strong upregulation of the IFN γ -regulated immune checkpoint Ido1 in Tyk2^{ΔIEC} tumors. The role of Ido1 in CRC and in cancer in general is not well defined, but several studies have reported an oncogenic activity. Kras^{G12D}-induced lung carcinogenesis and lung metastasis of orthotopically transplanted 4T1 mouse mammary cancer cells was reduced in Ido1 knockout mice.⁵¹ In addition, Ido1 knockout mice were resistant to skin cancer formation after DMBA/PMA treatment. In the DMBA/PMA model, Ido1 expression was induced by skin inflammation in a specific subset of plasmacytoid dendritic cells in the draining lymph nodes, which promoted immunosuppression and skin cancer formation.⁵² In contrast

to lung and skin carcinogenesis, formation of colitis-associated CRC was increased in Ido1 knockout mice after treatment with dimethylhydrazine and DSS, indicating a tumor-suppressive role.⁵³ However, a recent study showed that specific deletion of Ido1 in intestinal epithelial cells reduced AOM-DSS-induced colitis-associated CRC formation in mice.⁵⁴ These data revealed cell-type specific tumor promoting and tumor suppressing activities of Ido1 in colitis-associated CRC. We recently identified Ido1-expressing Paneth-like cancer cells in tumors of Apc^{Min} mice that prevent T cell infiltration and promote immune evasion. Ido-1 expression by these cells depends on Stat1 and IFN γ signaling.²⁸ Tyk2^{ΔIEC} tumors expressed higher levels of Stat1 and contained increased numbers of Ido1-expressing Paneth-like cancer cells. These cells may be responsible for reduced T cell infiltration in Tyk2^{ΔIEC}

tumors and allow tumor growth despite enhanced IFN γ signaling and intact immune surveillance. In contrast, IL12 and IFN γ signaling was attenuated in Tyk2 Δ/Δ tumors, resulting in impaired cancer immune surveillance with reduced NK cell and T cell infiltration. Ido1-expressing Paneth-like cancer cells were almost absent in Tyk2 Δ/Δ tumors and expression of antigen presentation machinery genes was reduced. This indicates that tumors in Tyk2 Δ/Δ are poorly immunoeedited and can progress to aggressive cancers without developing distinct immune evasion mechanisms.

Ido1 is the rate-limiting enzyme of the kynurenine pathway. It catalyzes oxidation of tryptophan to N-formylkynurenine, which is further converted to kynurenine and several kynurenine metabolites.⁵⁵ High Ido1 activity leads to tryptophan depletion and a corresponding increase of kynurenine metabolites. Tryptophan depletion negatively affects proliferation of effector T cells, while kynurenine promotes Treg differentiation via the aryl hydrocarbon receptor.^{56,57} Consequently, Ido1 creates an immunosuppressive microenvironment with reduced CD8⁺ T cell count and expansion of Tregs.^{58–60} Ido1 is frequently overexpressed in human CRC, which is associated with reduced levels of serum tryptophan and increased levels of kynurenine metabolites.^{61–63} In tumors, Ido1 is expressed by infiltrating myeloid cells and neoplastic epithelial cells.^{42,43,64} We have shown that the neoplastic epithelium of CRC is an important source of kynurenine.²⁸ Similarly, Ido1-expressing neoplastic epithelial cells of pancreatic ductal adenocarcinomas (PDACs) were critically involved in immune escape.⁶⁵ We have not performed metabolomics of mouse Tyk2-deficient CRCs. Ido1 expression was reduced in stromal immune cells but not in neoplastic cells of Tyk2 Δ/Δ tumors. In contrast, Ido1 expression was unaffected in stromal immune cells but increased in neoplastic cells of Tyk2 Δ^{IEC} tumors. Therefore, metabolomics of Tyk2 Δ/Δ and Tyk2 Δ^{IEC} would help to identify the main source of kynurenine metabolites in CRC.

The expression of several B cell markers such as CD19, CD20 and Pax5 was downregulated in Tyk2 Δ/Δ tumors. This suggests a lack of antigen-specific B cells, which would impair FC-mediated phagocytosis and antibody-dependent cellular cytotoxicity by NK cells. Alternatively, a previously identified cell population with dendritic cell characteristics but expressing the B cell markers CD19 and Pax5 could be reduced in Tyk2 Δ/Δ tumors. These B lymphoid-like cells are a major source of Ido1 in some tumors and have immunosuppressive activity on T cells.⁶⁶ Interestingly, the Ido1 pathway could also prevent complement deposition in tumors.⁵⁵ It has been shown that pharmacological or genetic Ido1 inhibition combined with chemo-radiotherapy resulted in extensive complement deposition in mouse brain tumors.⁶⁷ It is therefore possible that complement deposition is reduced in Tyk2 Δ/Δ tumors. Furthermore, expression of complement receptor 2, which is present on B cells and follicular dendritic cells, was also greatly reduced in Tyk2 Δ/Δ tumors, which could further impair complement-mediated anticancer immunity. In conclusion, we have identified a tumor-suppressive function of Tyk2 in stromal and CRC cells. Tyk2 blocks induction of the IFN γ -regulated immune checkpoint Ido1 in Paneth-like cancer cells by an unknown mechanism. Deletion of Tyk2 in Paneth-like cancer might change Jak-Stat signaling in a cell-intrinsic

manner. Stimulation with Jak-Stat-activating cytokines from the tumor microenvironment would enhance formation of Stat1-containing transcription factor complexes that lead to increased expression of type I and II interferon target genes including Ido1. The murine Ido1 promoter is not well characterized but the human Ido1 promoter contains multiple ISRE and GAS sites that respond to ISGF3 (Stat1-Stat2-IRF9) complexes and Stat1 homodimers, respectively.⁶⁸ An increased amount of such complexes in Tyk2-deficient Paneth-like cancer cells would enhance Ido1 expression. The generation of these cells could also be promoted in early neoplastic lesions of IBD patients by treatment with Tyk2 inhibitors, which would increase the risk of immune escape.

Materials and methods

Mice and in vivo experiments

Tyk2 $\Delta/+$, Tyk2 $^{fl/+}$, Villin-cre and Vav-cre mice have been described previously.^{69–71} Tyk2 $\Delta/+$ mice were generated by crossing Tyk2 $^{fl/+}$ mice with a CMV-cre germline deleter strain, which was then outcrossed. Tyk2 $\Delta/+$ mice were crossed to produce Tyk2 Δ/Δ and control Tyk2 $^{+/+}$ mice. Tyk2 $^{fl/fl}$ Villin-cre and Tyk2 $^{fl/fl}$ Vav-cre mice were crossed with Tyk2 $^{fl/fl}$ mice to generate cre-negative Tyk2 $^{fl/fl}$ control mice and cre-positive Tyk2 Δ^{IEC} and Tyk2 Δ^{Hem} mice. Mice were kept on a C57BL/6 genetic background and housed under standard conditions at the Dezentrale Biomedizinische Einrichtung of the Medical University Vienna. Autochthonous CRC development was induced using the AOM-DSS protocol.⁷² Mice were injected intraperitoneally with 12.5 mg/kg azoxymethane (AOM, Sigma, A5486) and, after 5 d of recovery, treated with two cycles of 2.5% dextrane sulfate salt (DSS, MP Biomedicals LCC, 160110) and one cycle of 2.0% DSS (w/v) via drinking water. DSS treatment lasted 5 d each with a 14-d interval of normal drinking water between cycles.⁷² After the last DSS cycle, mice recovered for 30 d before they were sacrificed. All mouse experiments were performed in accordance with Austrian and European laws and with the general regulations specified by the Good Scientific Practices guidelines of the Medical University of Vienna.

Genotyping by polymerase chain reaction (PCR)

Genotyping of Tyk2 was performed with 5'-GCAAGCCTGGTTACATGAG-3' and 5'-TGGACTGGAACCTGTGAGG A-3' primers. The Villin-Cre transgene was detected with 5'-CGGTCGATGCAACGAGTGATGAGG-3' and 5'-CCAGAG ACGGAAATCCATCGCTCG-3' primers. Vav-Cre genotyping was performed with 5'-TCAGAGTGAAGGACATCTCC CGCACC-3' and 5'-GTGGCAGAAGGGGCAGCCACACCA TT-3' primers.

Histochemistry, immunohistochemistry (IHC) and immunofluorescence (IF)

The colons of AOM-DSS-treated mice were isolated and flushed with phosphate-buffer saline (PBS) and fixed with 4% formaldehyde as “swiss rolls”. Tissues were embedded in

paraffin, cut into 4 μm thick sections tissue sections, deparaffinized in xylene and rehydrated in a decreasing ethanol series. Immunohistochemistry (IHC), immunofluorescence (IF) and hematoxylin & eosin (H&E) staining were performed using standard procedures.⁷² Briefly, for IHC and IF staining, antigen retrieval was performed using a pH6 citrate buffer or pH9 Tris-EDTA buffer depending on the antigen. For IHC staining, multiple blocking steps using hydrogen peroxide, avidin, biotin and the Mouse to Mouse HRP Staining System (ScyTek, MTM003-IFU) were performed. After blocking, the slides were stained using antibodies for BrdU (Abcam, ab6326), cleaved caspase 3 (Cell Signaling, 3700), Stat1 (Santa Cruz, sc-592), pStat1 (Cell Signaling, 9167), Stat3 (Santa Cruz, sc-7179), pStat3 (Cell Signaling, 9145), CD8 (Invitrogen, MA1-80231) and CD3 (Dako, A045229-2) in 1% BSA. IHC staining was detected with AEC substrate chromogen (Dako, K3464) or ImmPACT™ DAB Peroxidase Substrate Kit (VECSK-4105). Tissue sections for IF staining were blocked with 10% goat serum in PBS and incubated with primary antibodies for Ido1 (BioLegend, 654002), MMP7 (Cell Signaling, 3801) or E-cadherin (Abcam, ab11512) in 5% goat serum in PBS. The slides were incubated with fluorochrome-coupled secondary antibodies against rabbit (AF488, Fisher, A11034), mouse (Daylight649, BioLegend, 405312) or rat (Cy3, Fisher, A10522) immunoglobulins and counterstained with DAPI. For H&E staining, sections were incubated in hematoxylin for 10 min, dehydrated in an increasing ethanol series and stained with eosin for 2 min. For Alcian blue staining, the sections were incubated for 10 min each in Alcian blue and nuclear fast red. Stained “Swiss rolls” were scanned using a Panoramic Midi Slide Scanner (3D Histech, 40 \times objective) and staining intensities were analyzed with Definiens™ TissueStudio™ histomorphometry software (Definiens) as described previously.⁷²

Flow Cytometry

AOM-DSS-induced colorectal tumors from mice were pooled, minced and digested in 2 mL PBS containing 2% (v/v) FCS and 1 mg/mL collagenase IV (Life Technologies, 17104-019) for 45 min at 37°C under shaking. Afterward, the cells were strained through a 70 μm mesh and washed twice with 30 ml PBS. The cells were taken up in 200 μL of cell staining buffer and split in 4 equal parts. Extracellular stainings were performed using antibodies against 7-AAD (BioLegend, 420404), CD3 (BioLegend, B100305), CD4 (BioLegend, B116011), CD8a (BioLegend, B100737), CD45 (BioLegend, B103115), PD-1 (BioLegend, B135205), NK1.1 (BioLegend, B108739). For intracellular staining cells were fixed, permeabilized using the True nuclear TF staining buffer kit (BioLegend 424401) and stained with a FoxP3 (BioLegend, 126408) antibody. The data were collected using a FACS Fortessa (BD) and analyzed with FlowJo software.

RNA sequencing (RNA-seq)

RNA from AOM-DSS-induced macrodissected tumors was isolated using TRIzol Reagent (Thermo Fisher Scientific, 15596018) and purified using the RNeasy® Protect Mini Kit

(Qiagen, 74127) according to the manufacturer’s manual. RNA-sequencing was performed at the Core Facilities of the Medical University of Vienna. Sequencing libraries were prepared using the NEBNext Poly(A) mRNA Magnetic Isolation Module and the NEBNext Ultra™ II Directional RNA Library Prep Kit for Illumina according to manufacturer’s protocols (New England Biolabs). Libraries were QC-checked on a Bioanalyzer 2100 (Agilent) using a High Sensitivity DNA Kit for correct insert size and quantified using Qubit dsDNA HS Assay (Invitrogen). Pooled libraries were sequenced on a NextSeq500 instrument (Illumina) in 1x75bp single-end sequencing mode. Approximately 25 million reads were generated per sample. Reads in fastq format were aligned to the mouse reference genome version GRCh38⁷³ with Gencode mV23 annotations⁷⁴ using STAR aligner⁷⁵ version 2.6.1a in 2-pass mode. Reads per gene were counted by STAR, and differential gene expression was calculated using DESeq2⁷⁶ version 1.20.0. and analyzed using the Gene Set Enrichment Analysis (GSEA) tool provided by the Broad Institute.^{39,40}

Quantitative PCR (qPCR)

RNA from tissues and cells was isolated using TRIzol Reagent (Thermo Fisher Scientific, 15596018) and reverse transcribed using the QuantiTect Reverse Transcription Kit (Qiagen, 205313). For qPCR analysis, the GoTaq® qPCR Master Mix (Promega, A6001/2) and CFX96™ Real-Time System (Bio-Rad) were used with the following mouse primers:

GAPDH: 5'-TGTTTGTGATGGGTGTG-3', 5'-TACTTGGCAGGTTTCTC-3'; Tyk2_Exon3: 5'-CCCACAGGATGCTTGATGGT-3', 5'-CGACTTTGTGTGCGATGTGG-3'; Ido1: 5'-ATGTGGGCTTTGCTCTACCA-3', 5'-AAGCTGCCCGTCTCAATCA-3'; Tap1: 5'-ACCAGCTGTCAGGAGTTCAG-3', 5'-CTTGGGGCTCTCATAACAGGA-3'; Cxcl9: 5'-CGATCCA CTACAAATCCCTCA-3', 5'-TAGGCAGTTTATCTCCGT-3'; Ifi44: 5'-AGTCCTGTGAAGTCCAAGCTG-3', 5'-CAGCTGCCACTCTGAGACAT-3'.

Proteomics

Single AOM-DSS induced colorectal tumors from Tyk2 Δ/Δ , Tyk2 Δ^{IEC} mice and corresponding control mice were harvested, washed with PBS, snap frozen in liquid nitrogen (and stored at -80°C). Sample preparation and proteomics analysis were essentially performed as described before, with minor changes.⁷⁷ The tissue samples were separately homogenized in 130 μL lysis buffer (8 M urea, 50 mM TEAB, 5% SDS) using the Covaris S220 homogenizer. For enzymatic digestion, a protocol using the S-trap technology was employed.⁷⁸ Briefly, reduction and alkylation of 20 μg solubilized protein was achieved with 64 mM DTT and 48 mM IAA, respectively. After addition of trapping buffer (90%vol/vol methanol, 0.1 M triethylammonium bicarbonate), samples were loaded onto S-trap cartridges, thoroughly washed and subsequently digested using Trypsin/Lys-C Mix at 37°C for 2 h. Peptides were eluted, dried and stored at -20°C until LC-MS analyses. Dried samples were reconstituted in 5 μL of 30% FA containing 4 synthetic standard peptides and diluted with 40 μL of loading solvent (97.9% H₂O, 2% ACN, 0.05% trifluoroacetic acid). LC-MS/MS analyses were performed

using a Dionex Ultimate 3000 nano LC-system coupled to a timsTOF pro mass spectrometer (Bruker Daltonics). Five microliters of peptide solution were loaded on a 2 cm × 100 μm C18 Pepmap100 pre-column (Thermo) at a flow rate of 10 μl/min using mobile phase A. Afterward, peptides were eluted from the pre-column to a 25 cm × 75 μm 25 cm Aurora Series emitter column (Ionopticks) at a flow rate of 300 nL/min and separation was achieved using a gradient of 8% to 40% mobile phase B (79.9% acetonitrile, 20% H₂O, 0.1% FA) over 90 mins. Mass spectrometric analyses was accomplished using the timsTOF Pro mass spectrometer (Bruker) equipped with a captive spray ion source run at 1600 V. Furthermore, the timsTOF Pro mass spectrometer was operated in the Parallel Accumulation-Serial Fragmentation (PASEF) mode. Trapped ion mobility separation was achieved by applying a 1/kO scan range from 0.60–1.60 V.s/cm² resulting in a ramp time of 100 ms. All experiments were performed with ten PASEF MS/MS scans per cycle leading to a total cycle time of 1.16s. MS and MS/MS spectra were recorded using a scan range (m/z) from 100 to 1700. Furthermore, the collision energy was ramped as a function of increasing ion mobility from 20 to 52 eV and the quadrupole isolation width was set to 2 Th for m/z < 700 and 3 Th for m/z > 700.

MaxQuant 1.6.17.0⁷⁹ employing the Andromeda search engine was used for protein identification against the UniProt Database (version 12/2019 with 20.380 entries) allowing a mass tolerance of 20 ppm for MS spectra and 40 ppm for MS/MS spectra, an FDR <0.01 and a maximum of two missed cleavages. Furthermore, search criteria included carbamidomethylation of cysteine as fixed modification and methionine oxidation, N-terminal protein acetylation as variable modifications. Data evaluation was performed using the Perseus software V.1.6.14.0. Proteins that were detected in less than 70% of the samples were filtered out. Missing values from the remaining proteins were filled up according to a normal distribution with a width of 0.3 and a down shift of 1.8. The GOBPs were annotated using the integrated database of the Perseus software.

Statistics

All values are given as mean ± standard error of the mean (SEM). All data distributions were tested for normality using the Kolmogorov–Smirnov test. The calculation of significant differences between two groups was performed using unpaired *t*-test (for normal distributed data) and the Mann-Whitney test (for non-normal distributed data). Significant differences in tumor grading were calculated by performing a χ^2 -test. Significant differences between experimental groups were **p* < .05, ***p* < .01 and ****p* < .001.

Disclosure statement

No potential conflict of interest was reported by the author(s).

Funding

This work was supported by the Austrian Science Fund (FWF) SFB F6106 Doktoratskolleg-plus grant W1212-P21 (R.E.), the FWF Doc Fund DOC59-B33 (R.E.), the FWF standalone grants P35069-B (R.E.), P33430

and P32900 (E.C.), the Fellingner Cancer Research Foundation (D.H.-B.), and the FWF special research program grants SFB F6101 and F6106 (B.S., M.M.).

ORCID

Robert Eferl  <http://orcid.org/0000-0002-6074-7144>

Author contributions

Conceptualization, S.M. and R.E.;
Methodology, S.M., B.M., L.J., G.T. and D.H.-B.;
Investigation, S.M., B.M., I.S., D.Z. and L.K.;
Writing – Original Draft, S.M. and R.E.;
Writing – Review & Editing, S.M. and R.E.;
Resources, E.C., M.S., T.M., C.G., M.M. and B.S.

Data availability Statement

The data that support the findings of this study are available from the corresponding author upon reasonable request [<http://krebbsforschung.meduniwien.ac.at/forschung/forschungsschwerpunkte/zellulaere-und-molekulare-tumorbiologie/robert-eferl/>].

References

1. Siegel RL, Miller KD, Fuchs HE, Jemal A. Cancer statistics, 2022. *CA Cancer J Clin.* 2022;72(1):7–33. doi:10.3322/caac.21708.
2. Beaugerie L, Itzkowitz SH. Cancers complicating inflammatory bowel disease. *N Engl J Med.* 2015;372(15):1441–1452. doi:10.1056/NEJMra1403718.
3. Beaugerie L, Svrcek M, Seksik P, Bouvier A, Simon T, Allez M, Brixi H, Gornet J, Altwegg R, Beau P, et al. Risk of colorectal high-grade dysplasia and cancer in a prospective observational cohort of patients with inflammatory bowel disease. *Gastroenterology.* 2013;145(1):166–175 e168. doi:10.1053/j.gastro.2013.03.044.
4. Herrinton LJ, Liu L, Levin TR, Allison JE, Lewis JD, Velayos F. Incidence and mortality of colorectal adenocarcinoma in persons with inflammatory bowel disease from 1998 to 2010. *Gastroenterology.* 2012;143(2):382–389. doi:10.1053/j.gastro.2012.04.054.
5. Kim ER, Chang DK. Colorectal cancer in inflammatory bowel disease: the risk, pathogenesis, prevention and diagnosis. *World J Gastroenterol.* 2014;20(29):9872–9881. doi:10.3748/wjg.v20.i29.9872.
6. Pabla B, Bissonnette M, Konda VJ. Colon cancer and the epidermal growth factor receptor: current treatment paradigms, the importance of diet, and the role of chemoprevention. *World J Clin Oncol.* 2015;6(5):133–141. doi:10.5306/wjco.v6.i5.133.
7. Egan SE, Weinberg RA. The pathway to signal achievement. *Nature.* 1993;365(6449):781–783. doi:10.1038/365781a0.
8. Cantley LC. The phosphoinositide 3-kinase pathway. *Science.* 2002;296(5573):1655–1657. doi:10.1126/science.296.5573.1655.
9. Vivanco I, Sawyers CL. The phosphatidylinositol 3-Kinase AKT pathway in human cancer. *Nat Rev Cancer.* 2002;2(7):489–501. doi:10.1038/nrc839.
10. Domanska DBE, Domanska D. Review: the JAK/STAT protein activation – role in cancer development and targeted therapy. *Curr Signal Transduct Ther.* 2012;7(3):187–201. doi:10.2174/157436212802481619.
11. Yu H, Jove R. The STATs of cancer—new molecular targets come of age. *Nat Rev Cancer.* 2004;4(2):97–105. doi:10.1038/nrc1275.
12. Darnell JE Jr., Kerr IM, Stark GR. Jak-STAT pathways and transcriptional activation in response to IFNs and other extracellular signaling proteins. *Science.* 1994;264(5164):1415–1421. doi:10.1126/science.8197455.

13. Murray PJ. The JAK-STAT signaling pathway: input and output integration. *J Immunol.* 2007;178(5):2623–2629. doi:10.4049/jimmunol.178.5.2623.
14. Woss K, Simonovic N, Strobl B, Macho-Maschler S, Muller M. TYK2: an upstream kinase of STATs in cancer. *Cancers (Basel).* 2019;11(11):1728. doi:10.3390/cancers11111728.
15. Hu X, Li J, Fu M, Zhao X, Wang W. The JAK/STAT signaling pathway: from bench to clinic. *Signal Transduct Target Ther.* 2021;6(1):402. doi:10.1038/s41392-021-00791-1.
16. Strobl B, Stoiber D, Sexl V, Mueller M. Tyrosine kinase 2 (TYK2) in cytokine signalling and host immunity. *Front Biosci (Landmark Ed).* 2011;16(1):3214–3232. doi:10.2741/3908.
17. Levy DE, Darnell JE Jr. Stats: transcriptional control and biological impact. *Nat Rev Mol Cell Biol.* 2002;3(9):651–662. doi:10.1038/nrm909.
18. Ghoreschi K, Laurence A, O’Shea JJ. Janus kinases in immune cell signaling. *Immunol Rev.* 2009;228(1):273–287. doi:10.1111/j.1600-065X.2008.00754.x.
19. Raivola J, Haikarainen T, Abraham BG, Silvennoinen O. Janus Kinases in Leukemia. *Cancers (Basel).* 2021;13(4):800. doi:10.3390/cancers13040800.
20. Li B, Wan Q, Li Z, Chng WJ. Janus kinase signaling: oncogenic criminal of lymphoid cancers. *Cancers (Basel).* 2021;13(20):5147. doi:10.3390/cancers13205147.
21. Shahmarvand N, Nagy A, Shahryari J, Ohgami RS. Mutations in the signal transducer and activator of transcription family of genes in cancer. *Cancer Sci.* 2018;109(4):926–933. doi:10.1111/cas.13525.
22. Bromberg J, Darnell JE Jr. The role of STATs in transcriptional control and their impact on cellular function. *Oncogene.* 2000;19(21):2468–2473. doi:10.1038/sj.onc.1203476.
23. Bromberg JF, Horvath CM, Wen Z, Schreiber RD, Darnell JE Jr. Transcriptionally active Stat1 is required for the antiproliferative effects of both interferon alpha and interferon gamma. *Proc Natl Acad Sci U S A.* 1996;93(15):7673–7678. doi:10.1073/pnas.93.15.7673.
24. Shankaran V, Ikeda H, Bruce AT, White JM, Swanson PE, Old LJ, Schreiber RD. IFN γ and lymphocytes prevent primary tumour development and shape tumour immunogenicity. *Nature.* 2001;410(6832):1107–1111. doi:10.1038/35074122.
25. Bollrath J, Phesse TJ, von Burstin VA, Putoczki T, Bennecke M, Bateman T, Nebelsiek T, Lundgren-May T, Canli Ö, Schwitalla S, et al. gp130-mediated Stat3 activation in enterocytes regulates cell survival and cell-cycle progression during colitis-associated tumorigenesis. *Cancer Cell.* 2009;15(2):91–102. doi:10.1016/j.ccr.2009.01.002.
26. Musteanu M, Blaas L, Mair M, Schleder M, Bilban M, Tauber S, Esterbauer H, Mueller M, Casanova E, Kenner L, et al. Stat3 is a negative regulator of intestinal tumor progression in Apc(Min) mice. *Gastroenterology.* 2010;138(3):1003–1011 e1001–1005. doi:10.1053/j.gastro.2009.11.049.
27. Crnec I, Modak M, Gordziel C, Svinka J, Scharf I, Moritsch S, Pathria P, Schleder M, Kenner L, Timelthaler G, et al. STAT1 is a sex-specific tumor suppressor in colitis-associated colorectal cancer. *Mol Oncol.* 2018;12(4):514–528. doi:10.1002/1878-0261.12178.
28. Pflugler S, et al. IDO1(+) Paneth cells promote immune escape of colorectal cancer. *Commun Biol.* 2020;3(1):252. doi:10.1038/s42003-020-0989-y.
29. Tron AE, et al. Next-generation sequencing identifies a novel ELAVL1–TYK2 fusion gene in MOLM-16, an AML cell line highly sensitive to the PIM kinase inhibitor AZD1208. *Leuk Lymphoma.* 2016;57(12):2927–2929. doi:10.3109/10428194.2016.1171861.
30. Roberts KG, et al. Targetable kinase-activating lesions in Ph-like acute lymphoblastic leukemia. *N Engl J Med.* 2014;371(11):1005–1015. doi:10.1056/NEJMoa1403088.
31. Crescenzo R, Abate F, Lasorsa E, Tabbo’ F, Gaudio M, Chiesa N, Di Giacomo F, Spaccarotella E, Barbarossa L, Ercole E, et al. Convergent mutations and kinase fusions lead to oncogenic STAT3 activation in anaplastic large cell lymphoma. *Cancer Cell.* 2015;27(4):516–532. doi:10.1016/j.ccell.2015.03.006.
32. Velusamy T, Kiel MJ, Sahasrabudhe AA, Rolland D, Dixon CA, Bailey NG, Betz BL, Brown NA, Hristov AC, Wilcox RA, et al. A novel recurrent NPM1–TYK2 gene fusion in cutaneous CD30-positive lymphoproliferative disorders. *Blood.* 2014;124(25):3768–3771. doi:10.1182/blood-2014-07-588434.
33. Sanda T, et al. TYK2-STAT1–BCL2 pathway dependence in T-cell acute lymphoblastic leukemia. *Cancer Discov.* 2013;3(5):564–577. doi:10.1158/2159-8290.CD-12-0504.
34. Waanders E, Scheijen B, Jongmans MCJ, Venselaar H, van Reijmersdal SV, van Dijk AHA, Pastorczak A, Weren RDA, van der Schoot CE, van de Vorst M, et al. Germline activating TYK2 mutations in pediatric patients with two primary acute lymphoblastic leukemia occurrences. *Leukemia.* 2017;31(4):821–828. doi:10.1038/leu.2016.277.
35. Song XC, et al. Protein expression profiling of breast cancer cells by dissociable antibody microarray (DAMA) staining. *Mol Cell Proteomics.* 2008;7(1):163–169. doi:10.1074/mcp.M700115-MCP200.
36. Zhu X, Lv J, Yu L, Zhu X, Wu J, Zou S, Jiang S. Proteomic identification of differentially-expressed proteins in squamous cervical cancer. *Gynecol Oncol.* 2009;112(1):248–256. doi:10.1016/j.ygyno.2008.09.045.
37. Ide H, Nakagawa T, Terado Y, Kamiyama Y, Muto S, Horie S. Tyk2 expression and its signaling enhances the invasiveness of prostate cancer cells. *Biochem Biophys Res Commun.* 2008;369(2):292–296. doi:10.1016/j.bbrc.2007.08.160.
38. Kaminker JS, Zhang Y, Waugh A, Haverty PM, Peters B, Sebisano D, Stinson J, Forrest WF, Bazan JF, Seshagiri S, et al. Distinguishing cancer-associated missense mutations from common polymorphisms. *Cancer Res.* 2007;67(2):465–473. doi:10.1158/0008-5472.CAN-06-1736.
39. Subramanian A, Tamayo P, Mootha VK, Mukherjee S, Ebert BL, Gillette MA, Paulovich A, Pomeroy SL, Golub TR, Lander ES, et al. Gene set enrichment analysis: a knowledge-based approach for interpreting genome-wide expression profiles. *Proc Natl Acad Sci U S A.* 2005;102(43):15545–15550. doi:10.1073/pnas.0506580102.
40. Mootha VK, Lindgren CM, Eriksson K-F, Subramanian A, Sihag S, Lehar J, Puigserver P, Carlsson E, Ridderstråle M, Laurila E, et al. PGC-1 α -responsive genes involved in oxidative phosphorylation are coordinately downregulated in human diabetes. *Nat Genet.* 2003;34(3):267–273. doi:10.1038/ng1180.
41. van Baren N, Van den Eynde BJ. Tryptophan-degrading enzymes in tumoral immune resistance. *Front Immunol.* 2015;6(34). doi:10.3389/fimmu.2015.00034.
42. Ferdinande L, Decaestecker C, Verset L, Mathieu A, Moles Lopez X, Negulescu A-M, Van Maerken T, Salmon I, Cuvelier CA, Demetter P, et al. Clinicopathological significance of indoleamine 2,3-dioxygenase 1 expression in colorectal cancer. *Br J Cancer.* 2012;106(1):141–147. doi:10.1038/bjc.2011.513.
43. Uyttenhove C, Pilotte L, Théate I, Stroobant V, Colau D, Parmentier N, Boon T, Van den Eynde BJ. Evidence for a tumoral immune resistance mechanism based on tryptophan degradation by indoleamine 2,3-dioxygenase. *Nat Med.* 2003;9(10):1269–1274. doi:10.1038/nm934.
44. Simonovic N, Witalisz-Siepracka A, Meissl K, Lassnig C, Reichart U, Kolbe T, Farlik M, Bock C, Sexl V, Müller M, et al. NK cells require cell-extrinsic and -intrinsic TYK2 for full functionality in tumor surveillance and antibacterial immunity. *J Immunol.* 2019;202(6):1724–1734. doi:10.4049/jimmunol.1701649.
45. Prchal-Murphy M, Witalisz-Siepracka A, Bednarik KT, Putz EM, Gotthardt D, Meissl K, Sexl V, Müller M, Strobl B. In vivo tumor surveillance by NK cells requires TYK2 but not TYK2 kinase activity. *Oncoimmunology.* 2015;4(11):e1047579. doi:10.1080/2162402X.2015.1047579.
46. Stoiber D, Kovacic B, Schuster C, Schellack C, Karaghiosoff M, Kreibich R, Weisz E, Artwohl M, Kleine OC, Muller M, et al. TYK2 is a key regulator of the surveillance of B lymphoid tumors. *J Clin Invest.* 2004;114(11):1650–1658. doi:10.1172/JCI200422315.

47. Tokumasa N, Suto A, Kagami S-I, Furuta S, Hirose K, Watanabe N, Saito Y, Shimoda K, Iwamoto I, Nakajima H, et al. Expression of Tyk2 in dendritic cells is required for IL-12, IL-23, and IFN-gamma production and the induction of Th1 cell differentiation. *Blood*. 2007;110(2):553–560. doi:10.1182/blood-2006-11-059246.
48. Hainzl E, Stockinger S, Rauch I, Heider S, Berry D, Lassnig C, Schwab C, Rosebrock F, Milinovich G, Schleder M, et al. Intestinal epithelial cell tyrosine kinase 2 transduces IL-22 signals to protect from acute colitis. *J Immunol*. 2015;195(10):5011–5024. doi:10.4049/jimmunol.1402565.
49. Radwan M, Stiefvater R, Grunert T, Sharif O, Miller I, Marchetti-Deschmann M, Allmaier G, Gemeiner M, Knapp S, Kovarik P, et al. Tyrosine kinase 2 controls IL-1ss production at the translational level. *J Immunol*. 2010;185(6):3544–3553. doi:10.4049/jimmunol.0904000.
50. Zhang X, Wang S, Zhu Y, Zhang M, Zhao Y, Yan Z, Wang Q, Li X. Double-edged effects of interferons on the regulation of cancer-immunity cycle. *Oncoimmunology*. 2021;10(1929005). doi:10.1080/2162402X.2021.1929005.
51. Smith C, Chang MY, Parker KH, Beury DW, DuHadaway JB, Flick HE, Boulden J, Sutanto-Ward E, Soler AP, Laury-Kleintop LD, et al. IDO is a nodal pathogenic driver of lung cancer and metastasis development. *Cancer Discov*. 2012;2(8):722–735. doi:10.1158/2159-8290.cd-12-0014.
52. Muller AJ, Sharma MD, Chandler PR, DuHadaway JB, Everhart ME, Johnson BA, Kahler DJ, Pihkala J, Soler AP, Munn DH, et al. Chronic inflammation that facilitates tumor progression creates local immune suppression by inducing indoleamine 2,3 dioxygenase. *Proc Natl Acad Sci U S A*. 2008;105(44):17073–17078. doi:10.1073/pnas.0806173105.
53. Chang MY, Smith C, DuHadaway JB, Pyle JR, Boulden J, Soler AP, Muller AJ, Laury-Kleintop LD, Prendergast GC. Cardiac and gastrointestinal liabilities caused by deficiency in the immune modulatory enzyme indoleamine 2,3-dioxygenase. *Cancer Biol Ther*. 2011;12(12):1050–1058. doi:10.4161/cbt.12.12.18142.
54. Bishnupuri KS, Alvarado DM, Khouri AN, Shabsovich M, Chen B, Dieckgraefe BK, Ciorba MA. IDO1 and kynurenine pathway metabolites activate PI3K-Akt signaling in the neoplastic colon epithelium to promote cancer cell proliferation and inhibit apoptosis. *Cancer Res*. 2019;79(6):1138–1150. doi:10.1158/0008-5472.CAN-18-0668.
55. Munn DH, Mellor AL. IDO in the tumor microenvironment: inflammation, counter-regulation, and tolerance. *Trends Immunol*. 2016;37(3):193–207. doi:10.1016/j.it.2016.01.002.
56. Munn DH, et al. Inhibition of T cell proliferation by macrophage tryptophan catabolism. *J Exp Med*. 1999;189(9):1363–1372. doi:10.1084/jem.189.9.1363.
57. Mezrich JD, et al. An interaction between kynurenine and the aryl hydrocarbon receptor can generate regulatory T cells. *J Immunol*. 2010;185(6):3190–3198. doi:10.4049/jimmunol.0903670.
58. Holmgaard RB, et al. Tumor-expressed IDO recruits and activates MDSCs in a treg-dependent manner. *Cell Rep*. 2015;13(2):412–424. doi:10.1016/j.celrep.2015.08.077.
59. Prendergast GC, et al. Indoleamine 2,3-dioxygenase pathways of pathogenic inflammation and immune escape in cancer. *Cancer Immunol, Immunother: CII*. 2014;63(7):721–735. doi:10.1007/s00262-014-1549-4.
60. Zhai L, Spranger S, Binder DC, Gritsina G, Lauing KL, Giles FJ, Wainwright DA. Molecular pathways: targeting IDO1 and other tryptophan dioxygenases for cancer immunotherapy. *Clin Cancer Res*. 2015;21(24):5427–5433. doi:10.1158/1078-0432.ccr-15-0420.
61. Engin AB, Karahalil B, Karakaya AE, Engin A. *Helicobacter pylori* and serum kynurenine-tryptophan ratio in patients with colorectal cancer. *World J Gastroenterol*. 2015;21(12):3636–3643. doi:10.3748/wjg.v21.i12.3636.
62. Liu X, Shin N, Koblisch HK, Yang G, Wang Q, Wang K, Leffet L, Hansbury MJ, Thomas B, Rupar M, et al. Selective inhibition of IDO1 effectively regulates mediators of antitumor immunity. *Blood*. 2010;115(17):3520–3530. doi:10.1182/blood-2009-09-246124.
63. Walczak K, et al. Kynurenic acid synthesis and kynurenine aminotransferases expression in colon derived normal and cancer cells. *Scand J Gastroenterol*. 2011;46(7–8):903–912. doi:10.3109/00365521.2011.579159.
64. Théate I, et al. Extensive profiling of the expression of the indoleamine 2,3-dioxygenase 1 protein in normal and tumoral human tissues. *Cancer Immunol Res*. 2015;3(2):161–172. doi:10.1158/2326-6066.cir-14-0137.
65. Blair AB, et al. IDO1 inhibition potentiates vaccine-induced immunity against pancreatic adenocarcinoma. *J Clin Invest*. 2019;129(4):1742–1755. doi:10.1172/jci124077.
66. Johnson BA 3rd, et al. B-lymphoid cells with attributes of dendritic cells regulate T cells via indoleamine 2,3-dioxygenase. *Proc Natl Acad Sci U S A*. 2010;107(23):10644–10648. doi:10.1073/pnas.0914347107.
67. Li M, et al. The indoleamine 2,3-dioxygenase pathway controls complement-dependent enhancement of chemo-radiation therapy against murine glioblastoma. *J Immunother Cancer*. 2014;2(1):21. doi:10.1186/2051-1426-2-21.
68. Meireson A, Devos M, Brochez L. IDO expression in cancer: different compartment, different functionality? *Front Immunol*. 2020;11:531491. doi:10.3389/fimmu.2020.531491.
69. de Boer J, Williams A, Skavdis G, Harker N, Coles M, Tolaini M, Norton T, Williams K, Roderick K, Potocnik A, et al. Transgenic mice with hematopoietic and lymphoid specific expression of Cre. *Eur J Immunol*. 2003;33(2):314–325. doi:10.1002/immu.200310005.
70. El Marjou F, et al. Tissue-specific and inducible Cre-mediated recombination in the gut epithelium. *Genesis*. 2004;39(3):186–193. doi:10.1002/gene.20042.
71. Vielmascher RM, Hainzl E, Leitner NR, Rammerstorfer M, Popp D, Witalisz A, Rom R, Karaghiosoff M, Kolbe T, Müller S, et al. Conditional ablation of TYK2 in immunity to viral infection and tumor surveillance. *Transgenic Res*. 2014;23(3):519–529. doi:10.1007/s11248-014-9795-y.
72. Crncec I, Pathria P, Svinka J, Eferl R. Induction of colorectal cancer in mice and histomorphometric evaluation of tumors. *Methods Mol Biol*. 2015;1267:145–164. doi:10.1007/978-1-4939-2297-0_7.
73. *mm10 murine reference genome database downloaded from Ensembl*, ftp://ftp.ensembl.org/pub/release-93/fasta/mus_musculus/dna/Mus_musculus.GRCm38.dna_sm.primary_assembly.fa.gz
74. *Murine genome annotations downloaded from Gencode*, ftp://ftp.ebi.ac.uk/pub/databases/gencode/Gencode_mouse/release_M23/gencode.vM23.chr_patch_hapl_scaff.annotation.gtf.gz
75. Dobin A, Davis CA, Schlesinger F, Drenkow J, Zaleski C, Jha S, Batut P, Chaisson M, Gingeras TR. STAR: ultrafast universal RNA-seq aligner. *Bioinformatics*. 2013;29(1):15–21. doi:10.1093/bioinformatics/bts635.
76. Love MI, Huber W, Anders S. Moderated estimation of fold change and dispersion for RNA-seq data with DESeq2. *Genome Biol*. 2014;15(12):550. doi:10.1186/s13059-014-0550-8.
77. Bileck A, Bortel P, Kriz M, Janker L, Kiss E, Gerner C, Del Favero G. Inward outward signaling in ovarian cancer: morpho-phospho-proteomic profiling upon application of hypoxia and shear stress characterizes the adaptive plasticity of OVCAR-3 and SKOV-3 cells. *Front Oncol*. 2021;11:746411. doi:10.3389/fonc.2021.746411.
78. Zougman A, Selby PJ, Banks RE. Suspension trapping (STrap) sample preparation method for bottom-up proteomics analysis. *Proteomics*. 2014;14(9):1000–1006. doi:10.1002/pmic.201300553.
79. Tyanova S, Temu T, Cox J. The MaxQuant computational platform for mass spectrometry-based shotgun proteomics. *Nat Protoc*. 2016;11(12):2301–2319. doi:10.1038/nprot.2016.136.